# Upper-Tropospheric Synoptic-Scale Waves. Part II: Maintenance and Excitation of Quasi Modes

CHANTAL RIVEST

*Center for Meteorology and Physical Oceanography, Massachusetts Institute of Technology, Cambridge, Massachusetts*

BRIAN F. FARRELL

*Harvard University, Department of Earth and Planetary Sciences, Cambridge, Massachusetts*

(Manuscript received 7 October 1991, in final form 20 February 1992)

ABSTRACT

In a preceding paper a simple dynamical model for the maintenance of upper-tropospheric waves was proposed: the upper-level Eady normal modes. In this paper it is shown that these modes have counterparts in basic states with positive tropospheric gradients of potential vorticity, and that these counterparts can be maintained and excited on time scales consistent with observations.

In the presence of infinitesimal positive tropospheric gradients of potential vorticity, the upper-level normal-mode solutions no longer exist. That the normal-mode solution disappears when gradients are infinitesimal represents an apparent singularity and challenges the interpretation of upper-level synoptic-scale waves as related to the upper-level Eady normal modes. What happens to the upper-level modal solution in the presence of tropospheric gradients of potential vorticity is examined in a series of initial-value experiments. Our results show that they become slowly decaying quasi modes. Mathematically the quasi modes consist of a superposition of singular modes sharply peaked in the phase speed domain, and their decay proceeds as the modes interfere with one another. We repeat these experiments in basic states with a smooth tropopause in the presence of tropospheric and stratospheric gradients, and similar results are obtained.

Following a previous study by Farrell, a class of near-optimal initial conditions for the excitation of upper-level waves is identified. The initial conditions consist of upper-tropospheric disturbances that lean against the shear. They strongly excite upper-level waves not only in the absence of tropospheric potential vorticity gradients, but also in their presence. This result is important mathematically since it suggests that quasi modes are as likely to emerge from favorably configured initial disturbances as true normal modes, although the excitation is followed by a slow decay.

## 1. Introduction

We have previously proposed a simple dynamical model for the maintenance of upper-tropospheric synoptic-scale waves in midlatitudes based on the upper-level Eady normal modes (Rivest et al. 1992; Part I of this paper). However, a potential objection to this interpretation remains, arising from the fact that the modal solutions cease to exist in the presence of positive tropospheric gradients of potential vorticity, as was demonstrated in Green (1960). In this paper we show that the upper-level normal modes have counterparts in basic states with potential vorticity gradients and that these counterparts can be maintained and excited on time scales consistent with observations of upper-level waves (Sanders 1988).

As a first step, we perform a series of initial-value experiments and observe what happens to the upper-level normal mode in the presence of positive tropospheric gradients of potential vorticity. We then study the mathematical structure of these upper-level waves. Since the basic-state gradient of quasigeostrophic potential vorticity (QPV) is one-signed, they cannot be unstable modes (Charney and Stern 1962). Furthermore, an argument of Bretherton (1966) rules out the possibility of their existence as neutral modes. However, we show that, even in the absence of neutral and unstable normal modes, the basic states examined here support quasi modes. Stationary quasi modes in shear flows have been discussed previously in Held et al. (1985). This paper represents the first study on propagating quasi modes.

The quasi modes consist of a superposition of singular neutral modes with a distribution sharply peaked in the phase speed domain. The decay of the quasi modes does not proceed as $1/t$, as would be expected for the Couette problem in the asymptotic limit $t \to \infty$ (Case 1960). Instead, the streamfunction field displays behavior more typical of slowly decaying normal

Present affiliation: Division de Recherche en Prévision Numérique, Atmospheric Environment Service, Canada.

*Corresponding author address:* Dr. Chantal Rivest, Atmospheric Environment Service, Division de Recherche en Prévision Numérique, 2121 Route Transcanadienne, Dorval, H9P 1J3 PQ Canada.

modes. In the limit $\beta \to 0$, the distribution approaches a Kronecker delta and corresponds to a neutral normal-mode solution. As $\beta$ increases from 0, the distribution widens, and the streamfunction amplitude and the total perturbation energy decay more rapidly with time.

The parameter dependency of the exponential decay rate of the quasi modes, $\Lambda$, obeys the following proportionality relationship, $\Lambda \propto \beta k/(k^2 + l^2)$, as was suggested by the approximate calculation in Part I. Meridionally elongated waves are found to decay faster than zonally elongated waves, consistently with the fact that the meridional QPV gradient, $Q_y$, is advected by the meridional wind, which is itself proportional to the zonal wavenumber. The effect of decaying quasi modes on the mean flow is also studied. In contrast to low-level Charney waves that tend to erase both meridional gradients of surface temperature and interior QPV in the middle of the channel (Edmon et al. 1980), quasi modes act to enhance temperature gradients at the upper boundary while decreasing interior QPV gradients.

As a second step, we study the excitation of upper-level waves. In the paradigm of linear waves embedded in unstable basic states, growth at upper levels seems to be favored by weak low-level baroclinicity, boundary-layer friction, and a tropopause (Snyder and Lindzen 1988; Whitaker and Barcilon 1992). We argue that the weak low-level baroclinicity is not necessarily typical for upper-level growth and also that realistic meridional structure leads to unstable waves with zonal wavelengths that are too large compared to the observations of 2500 km (Sanders 1988).

We follow here a different approach to the problem of the origin of upper-level waves (Farrell 1989), identifying a class of near-optimal initial conditions for their excitation. These initial conditions consist of upper-tropospheric disturbances that typically lean against the shear. They strongly excite upper-level waves even in the presence of tropospheric potential vorticity gradients. This result is important mathematically since it demonstrates that quasi modes are as likely to emerge from favorably configured initial disturbances as modal waves, even if the excitation is followed by slow decay in the former case.

The paper is organized as follows. In section 2 the necessary mathematical information is presented; section 3 contains a comprehensive discussion of the quasi modes; in section 4 we present the excitation of the quasi modes in a basic-state flow characteristic of the midlatitude flow; and finally, the conclusions are summarized in section 5.

## 2. Mathematical formulation

### a. *Quasigeostrophic dynamics in a basic-state flow*

We choose the quasigeostrophic set of equations to model the dynamics of upper-level synoptic-scale waves (Pedlosky 1979).

Let us consider perturbations $[q, \psi, u, v, w, \theta]$ $(x, y, z, t)$ in a basic-state flow $[Q, \Psi, U, \Theta](y, z)$, where $Q + q$ is the total quasigeostrophic pseudo-potential vorticity, $\Psi + \psi$ the geostrophic streamfunction, $U + u$ the zonal geostrophic wind, $v$ the meridional geostrophic wind, $w$ the vertical velocity, $\Theta + \theta$ the potential temperature, and where $(x, y, z, t)$ are the zonal, meridional, vertical, and time coordinates. The nondimensional equations for the basic state are

$$Q_y = \beta - \left[\frac{\partial^2}{\partial y^2} + \frac{1}{\rho}\frac{\partial}{\partial z}\left(\frac{\rho}{N^2}\frac{\partial}{\partial z}\right)\right]U, \tag{1}$$

$$U = -\frac{\partial \Psi}{\partial y}, \tag{2}$$

$$\Theta = \frac{\partial \Psi}{\partial z}; \tag{3}$$

and for the perturbation fields:

$$\left[\frac{\partial}{\partial t} + U\frac{\partial}{\partial x} + J(\psi, )\right]q = -Q_y\frac{\partial \psi}{\partial x}, \tag{4}$$

$$\left[\frac{\partial}{\partial t} + U\frac{\partial}{\partial x} + J(\psi, )\right]\theta = -N^2 w - \Theta_y\frac{\partial \psi}{\partial x}, \tag{5}$$

where

$$q = \left[\nabla_H^2 + \frac{1}{\rho}\frac{\partial}{\partial z}\left(\frac{\rho}{N^2}\frac{\partial}{\partial z}\right)\right]\psi, \tag{6}$$

$$u = -\frac{\partial \psi}{\partial y}, \quad v = \frac{\partial \psi}{\partial x}, \quad \theta = \frac{\partial \psi}{\partial z}, \tag{7}$$

$$J(A, B) \equiv A_x B_y - A_y B_x,$$

$$\nabla_H^2 \equiv \frac{\partial^2}{\partial x^2} + \frac{\partial^2}{\partial y^2};$$

$N^2(z)$ is the reference static stability profile, $\rho(z)$ is the reference density profile, and $\beta$ the latitudinal gradient of planetary vorticity.

For a selected vertical scale, $H$, an associated horizontal scale, $L \equiv N_0 H/f_0$, follows. In addition we choose a velocity scale, $U_0$, a reference static stability $N_0$, potential temperature $\theta_0$, and density $\rho_0$, and an average planetary vorticity, $f_0$. We can then recover the dimensional variables and parameters (that are primed):

$$(x', y', z') = L\left(x, y, \frac{H}{L}z\right), \quad t' = \frac{L}{U_0}t,$$

$$N' = N_0 N, \quad \rho' = \rho_0 \rho,$$

$$(Q', q') = \mathrm{Ro}\, f_0 (Q, q),$$

$$(\Psi', \psi') = U_0 L(\Psi, \psi),$$

$$(U', u', v') = U_0 (U, u, v),$$

$$(\Theta', \theta') = \theta_0 \frac{f_0 L U_0}{gH} (\Theta, \theta),$$

$$w' = \mathrm{Ro} \frac{H}{L} U_0 w, \quad \beta' = \frac{\beta U_0}{L^2}, \tag{8}$$

where Ro is the Rossby number, $\mathrm{Ro} \equiv U_0/Lf_0$.

*b. Linear waves in a zonal channel*

We consider linear waves confined in a zonal channel, with basic-state winds having no meridional dependency. Such basic-state flows lead to perturbation fields that are separable in $y$ and $z$. However, we do not impose here modal solutions and assume separability of the vertical and time structures.

We assume a density profile that decays exponentially with height throughout the domain,

$$\rho = \exp[-sz]. \tag{9}$$

From (1), (2), and (3) the basic-state equations are

$$Q_y = \beta - \frac{1}{\rho}\frac{d}{dz}\left(\frac{\rho}{N^2}\frac{dU}{dz}\right) = \beta + \frac{s_N}{N^2}\frac{dU}{dz} - \frac{1}{N^2}\frac{d^2U}{dz^2}, \tag{10}$$

$$\Psi = -U(z)y, \tag{11}$$

$$\Theta = \frac{\partial \Psi}{\partial z}, \tag{12}$$

where

$$s_N = s + \frac{1}{N^2}\frac{dN^2}{dz}. \tag{13}$$

For perturbation fields of the form,

$$[q, \psi, v, w, \theta](x, y, z, t) = \mathrm{Re}([\tilde{q}, \tilde{\psi}, \tilde{v}, \tilde{w}, \tilde{\theta}](z, t)e^{ikx}) \sin ly,$$

$$u(x, y, z, t) = \mathrm{Re}(\tilde{u}(z, t)e^{ikx}) \cos ly, \tag{14}$$

where $l = \pi/L_y$, $k = 2\pi/L_x$, $L_y$ is the channel width, and $L_x$ the zonal wavelength, the linear equations (4), (5), (6), and (7) are

$$\left[\frac{\partial}{\partial t} + ikU\right]\tilde{q} = -ikQ_y\tilde{\psi}, \tag{15}$$

$$\left[\frac{\partial}{\partial t} + ikU\right]\frac{\partial \tilde{\psi}}{\partial z} = -N^2\tilde{w} - ik\Theta_y\tilde{\psi}, \tag{16}$$

where

$$\tilde{q} = \left[-K^2 - \frac{s_N}{N^2}\frac{\partial}{\partial z} + \frac{1}{N^2}\frac{\partial^2}{\partial z^2}\right]\tilde{\psi}, \tag{17}$$

$$\tilde{u} = -l\tilde{\psi}, \quad \tilde{v} = ik\tilde{\psi}, \quad \tilde{\theta} = \frac{\partial \tilde{\psi}}{\partial z}, \tag{18}$$

and $K$ is the total horizontal wavenumber, $K^2 = k^2 + l^2$.

The equations presented so far need to be completed by suitable boundary conditions in the vertical: at the inviscid upper and lower horizontal boundaries, $z = z_u$ and $z = z_l$,

$$\tilde{w} = 0. \tag{19}$$

Substituting $\tilde{w}$ from (16) yields

$$\left[\frac{\partial}{\partial t} + ikU\right]\frac{\partial \tilde{\psi}}{\partial z} + ik\Theta_y\tilde{\psi} = 0 \quad \text{at} \quad z = z_l, \tag{20}$$

$$\left[\frac{\partial}{\partial t} + ikU\right]\frac{\partial \tilde{\psi}}{\partial z} + ik\Theta_y\tilde{\psi} = 0 \quad \text{at} \quad z = z_u. \tag{21}$$

In the following sections we are also going to consider semi-infinite vertical domains and use approximate boundary conditions. Derivation of these boundary conditions is straightforward (Béland and Warn 1975; Rasch 1986). In the case of a semi-infinite atmosphere $-\infty < z < z_u$, the following boundedness boundary condition holds at $z = z_l$:

$$\frac{\partial}{\partial t}\left[\frac{\partial \tilde{\psi}}{\partial z} - (s/2 + \chi_l)\tilde{\psi}\right] = -ikU_l\left[\frac{\partial \tilde{\psi}}{\partial z} - (s/2 - \chi_l)\tilde{\psi}\right] - \frac{ik\beta N_l^2}{2\chi_l}\tilde{\psi}. \tag{22}$$

and in the case of a semi-infinite atmosphere $z_l < z < \infty$, the following one at $z = z_u$:

$$\frac{\partial}{\partial t}\left[\frac{\partial \tilde{\psi}}{\partial z} - (s/2 - \chi_u)\tilde{\psi}\right] = -ikU_u\left[\frac{\partial \tilde{\psi}}{\partial z} - (s/2 - \chi_u)\tilde{\psi}\right] + \frac{ik\beta N_u^2}{2\chi_u}\tilde{\psi}, \tag{23}$$

where

$$\chi_l^2 = N_l^2K^2 + s^2/4, \quad \chi_u^2 = N_u^2K^2 + s^2/4,$$

and $U_l$, $N_l^2$, and $U_u$, $N_u^2$ are values at the lower and upper boundaries, respectively.

The equations (15) accompanied by (17) with the set of boundary conditions (20) or (22), and (21) or (23), represent an initial-value problem for $\tilde{\psi}(z)$, given the initial condition $\tilde{\psi}_0(z)$.

This system has the property that the basic-state flow and the perturbation can exchange energy, regardless of whether unstable modes exist or not. We define the total perturbation energy, $E_T$, as the sum of the potential and kinetic energy,

$$E_T = \int_{z_l}^{z_u}\int_0^{L_y} dydz \times \frac{\rho}{2}\overline{\left[\left(\frac{\partial \psi}{\partial x}\right)^2 + \left(\frac{\partial \psi}{\partial y}\right)^2 + \frac{1}{N^2}\left(\frac{\partial \psi}{\partial z}\right)^2\right]}, \tag{24}$$

TABLE 1. Dimensional and nondimensional variables; $Z'$ is the height at a pressure surface typical of the tropopause, and $P'$ is the pressure at the ground.

| |
|---|
| $(x', y') = 900$ km $(x, y)$ |
| $(z') = 9$ km $(z)$ |
| $(t') = .39$ day $(t)$ |
| $(Z'(z = 1)) = 24$ dm $(\psi)$ |
| $(P'(z = 0)) = 24$ hPa $(\psi)$ |
| $(U', u', v') = 27$ m s$^{-1}$ $(U, u, v)$ |
| $(\Theta', \theta') = 8.1$ K $(\Theta, \theta)$ |
| $(w') = 8.1$ cm s$^{-1}$ $(w)$ |

where

$$\overline{(\ )} = \frac{1}{L_x}\int_0^{L_x} dx(\ ). \tag{25}$$

From (4) and (5) we obtain, in the absence of friction,

$$\frac{dE_T}{dt} = -\int_{z_l}^{z_u}\int_0^{L_y} dydz\,\frac{\rho U_z}{N^2}\,\overline{\frac{\partial\psi}{\partial x}\frac{\partial\psi}{\partial z}}. \tag{26}$$

When the perturbation streamfunction tilts upshear with height in average, the right-hand side of (26) is positive and the perturbation energy increases with time, whereas when it tilts downshear, the perturbation energy decreases with time. When the perturbation gains energy, the mean flow loses the same amount, as the linear problem is energetically consistent. However, the effect of this feedback on the mean is not, in general, considered in linear dynamics.

### c. *Modal decomposition*

If we express

$$\tilde{\psi}(z, t) = \hat{\psi}_i(z)e^{-ikc_it}$$

in (15), (17), (20) or (22), and (21) or (23), we get the equations for the modes of the system, discrete and continuous, where $\hat{\psi}_i(z)$ correspond to the eigenvectors and $c_i$ to their associated eigenvalues (Farrell 1982, 1989). After discretization, it is possible to express these equations in a matrix form:

$$A\hat{\psi}_i = c_i\hat{\psi}_i,$$

where $A$ is a matrix operator that approaches the differential dynamical operator in the continuous limit.

Let us look at the Hermitian transpose linear system,

$$A^H\hat{\psi}^a_m = d_m\hat{\psi}^a_m,$$

where $A^H$ is the Hermitian transpose of $A$, and $d_m$ the eigenvalue associated with the $m$th eigenvector, $\hat{\psi}^a_m$. The Hermitian transpose matrix corresponds in the continuous limit to the adjoint differential operator. See Ince (1926) for a discussion of differential operators and their adjoint. It is easy to show that

$$d_m = c^*_m,$$

where the * refers to the complex conjugate, and that a special biorthogonality relationship links the modes of the system and its Hermitian transpose,

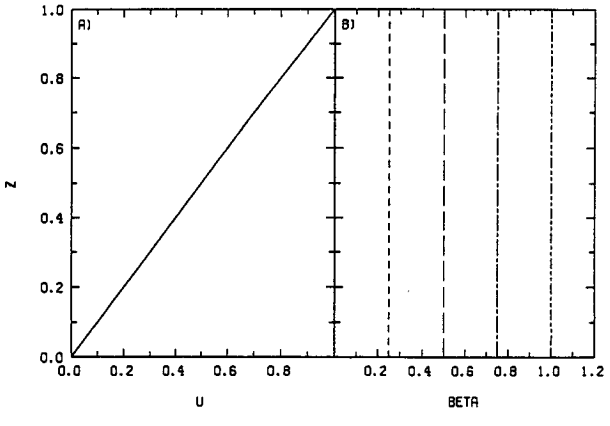


FIG. 1. The vertical profiles of basic state (a) wind $U(z)$ and (b) QPV gradient $Q_y(z)$. In (b), $\beta = 0.25$ (short-dash line), 0.5 (long-dash line), 0.75 (long-dash–short-dash line), and 1 (long-dash–double short-dash line).

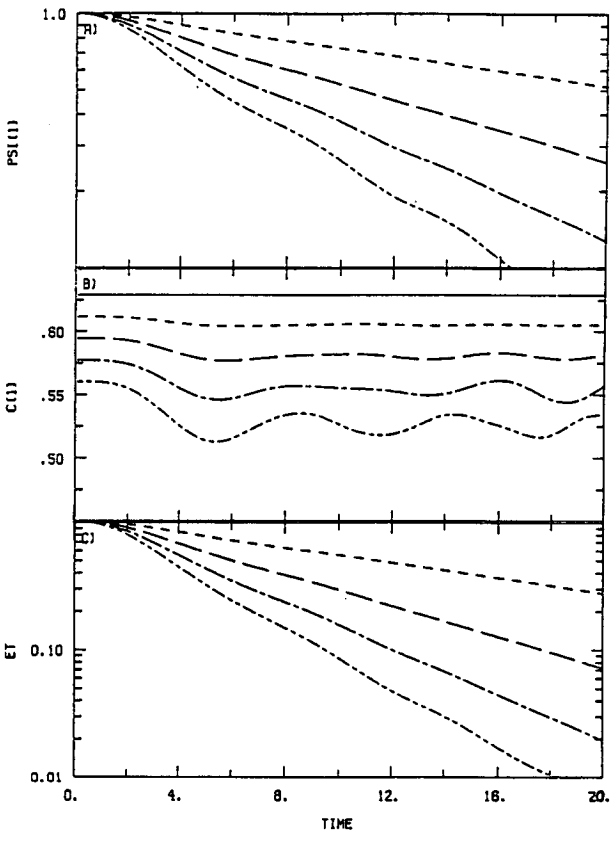


FIG. 2. Time series of (a) $|\tilde{\psi}|^{z=1}$, (b) $c|^{z=1}$, and (c) $E_T$ for initial-value experiments with $k = 2.3$, $l = 1.4$, and variable $\beta$. $\beta = 0$ (solid line), 0.25 (short-dash line), 0.5 (long-dash line), 0.75 (long-dash–short-dash line), and 1 (long-dash–double short-dash line). Initial streamfunction amplitude is fixed to unity at the lid, and $E_T$ is normalized by its initial value.

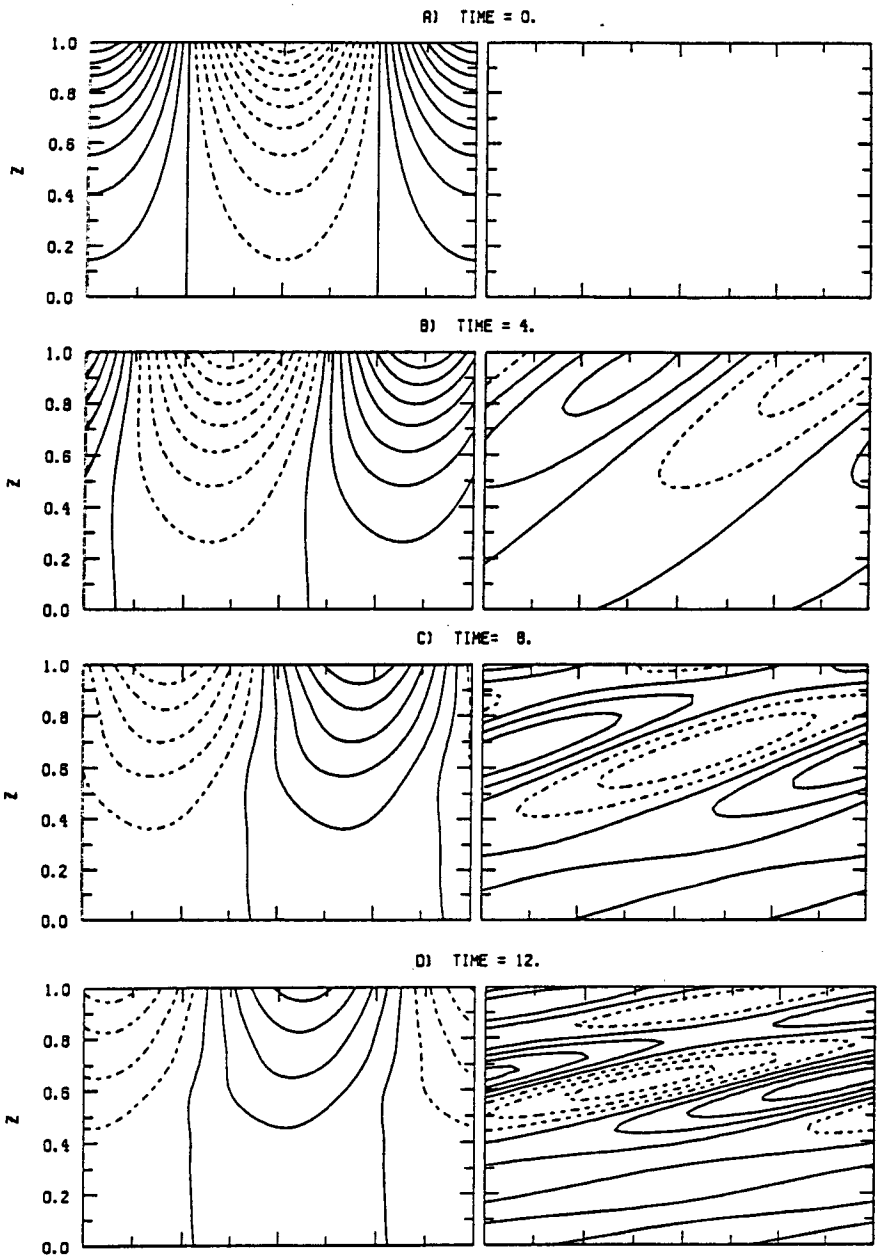


FIG. 3. Time evolution of the midchannel perturbation streamfunction and QPV fields for the initial-value experiment with $k = 2.3$, $l = 1.4$, and $\beta = 0.5$. Time = (a) 0, (b) 4, (c) 8, (d) 12. The contour interval is 0.1 for the streamfunction, and 1 for the QPV. Negative values are dashed. A full zonal wavelength is represented.

$$\frac{(\hat{\psi}_m^a, \hat{\psi}_j)}{(\hat{\psi}_j^a, \hat{\psi}_j)} = \delta_{mj}, \tag{27}$$

where $\delta_{mj}$ is the function of Kroenecker, and where we have defined an inner product:

$$(\psi^a, \psi) = \sum_{k=1}^{N} \psi_k^a \psi_k.$$

Once both the modes of the system and of its Hermitian transpose are known, the initial-value problem can easily be solved. The modes $\hat{\psi}_j$ form a complete set, and the solution can be expressed as

$$\tilde{\psi}(z, t) = \sum_{j=1}^{N} a_j \hat{\psi}_j e^{-ikc_j t}. \tag{28}$$

For a given initial condition, $\psi_0$, the coefficients $a_j$ can be determined with the biorthogonality relationship,

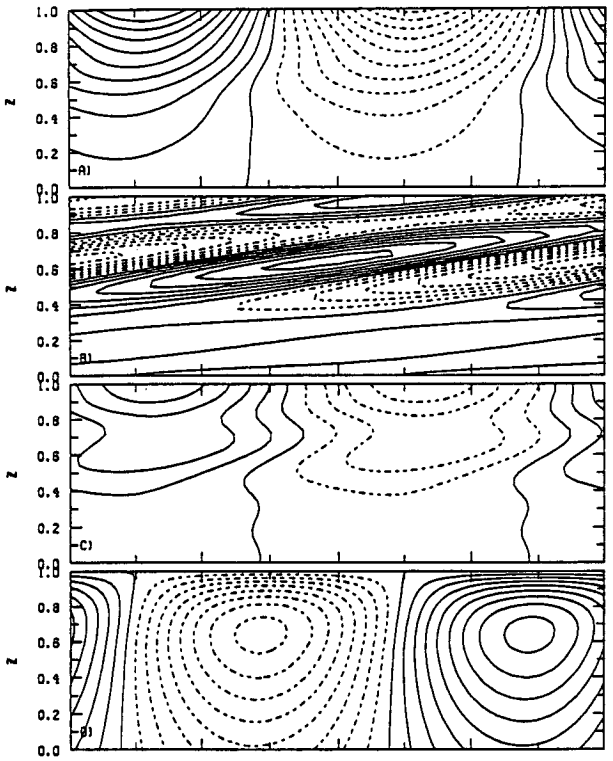

FIG. 4. Midchannel $x$–$z$ cross section of perturbation fields for the initial-value experiment with $k = 2.3$, $l = 1.4$, and $\beta = 0.5$, at time = 10. (a) Streamfunction, (b) QPV, (c) potential temperature, and (d) vertical velocity. The contour interval is 0.05 in (a), 0.5 in (b), 0.25 in (c), and 0.05 in (d). Negative values are dashed. A full zonal wavelength is represented.

$$a_j = \frac{(\hat{\psi}_j^a, \psi_0)}{(\hat{\psi}_j^a, \hat{\psi}_j)}.$$

Farrell (1982, 1989) used this technique to solve the initial-value problem. The important mechanism in (28) is the interference between the nonorthogonal modes. The total energy is then not the sum of the individual modal energies. Effects of this kind are discussed in Lindzen et al. (1982) and Rotunno and Fantini (1989), where the interference takes place between two discrete modes.

### d. Parameter values

In this paper, we are concerned with synoptic-scale motions in the region of the jet. We choose $f_0 = 10^{-4}\,\mathrm{s}^{-1}$, $g = 10\ \mathrm{m\,s}^{-2}$, $N_0 = 10^{-2}\,\mathrm{s}^{-2}$, $\beta' = 1.6 \cdot 10^{-11}\ \mathrm{m\,s}^{-1}$, and $H = 9$ km, roughly the tropopause height in the middle of the jet. This value of $H$ implies a Rossby radius, $L = 900$ km. Also, we take $U_0 = \gamma_0 H$, where $\gamma_0$ is an average tropospheric shear so that fixing $\gamma_0 = 3\,(\mathrm{m\,s}^{-1})/\mathrm{km}$ yields $U_0 = 27\ \mathrm{m\,s}^{-1}$. For these values the nondimensional beta and the Rossby number are: $\beta = 0.5$ and Ro = 0.3. Table 1 summarizes the correspondence between dimensional and nondimensional variables. We consider a channel with $l = 1.4$, that is, of nondimensional and dimensional widths $L_y = 2.2$ and $L'_y = 2000$ km (from Table 1).

## 3. The quasi modes

### a. Basic states

We consider in this section a Boussinesq fluid, $s = 0$ and $\rho = 1$, and basic states with constant shear $U(z) = z$ and constant static stability $N^2 = 1$. From (10) the meridional QPV gradient reduces to $Q_y = \beta$. We assume a semi-infinite domain bounded by an inviscid rigid lid at $z_u = 1$. The assumption is valid for upper-tropospheric waves since we saw in Part I that at the scales considered their dynamics at $z = 0$ is quite the same whether there is a lower boundary or not. Figure 1 displays the vertical profiles of basic-state wind and meridional QPV gradient. From Table 1 these nondimensional values correspond to a basic-state wind at the lid (or rigid tropopause) of 27 m s$^{-1}$, with a temperature change across the channel of 18°C, and to a tropospheric static stability of $10^{-4}\,\mathrm{s}^{-2}$. Recall from

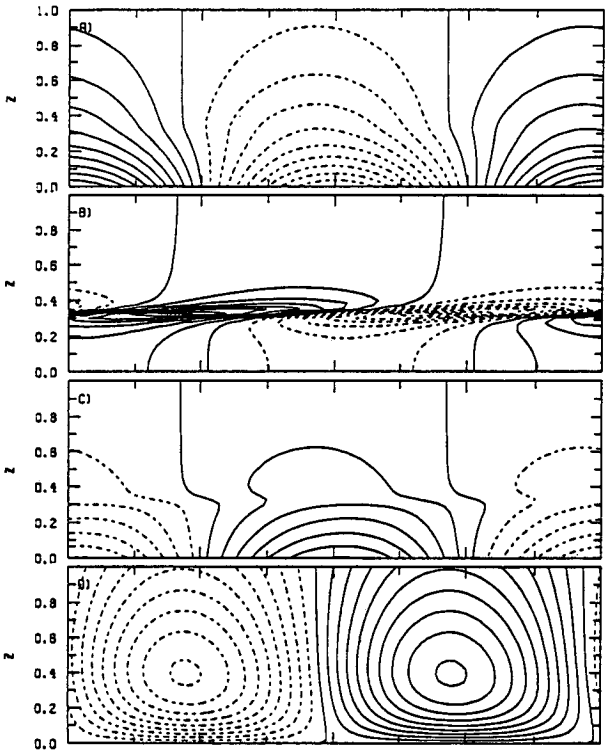

FIG. 5. Midchannel $x$–$z$ cross section of perturbation fields for the lower-level Charney mode with $s = 0$, $k = 2.3$, $l = 1.4$, and $\beta = 0.5$. (a) Streamfunction, (b) QPV, (c) potential temperature, and (d) vertical velocity. Maximum streamfunction amplitude is fixed to unity. The contour interval is 0.1 in (a), 1 in (b), 0.5 in (c), and 0.1 in (d). Negative values are dashed. A full zonal wavelength is represented. Note that the ratios between the different contour intervals are the same as in Fig. 4, so that they can be compared.

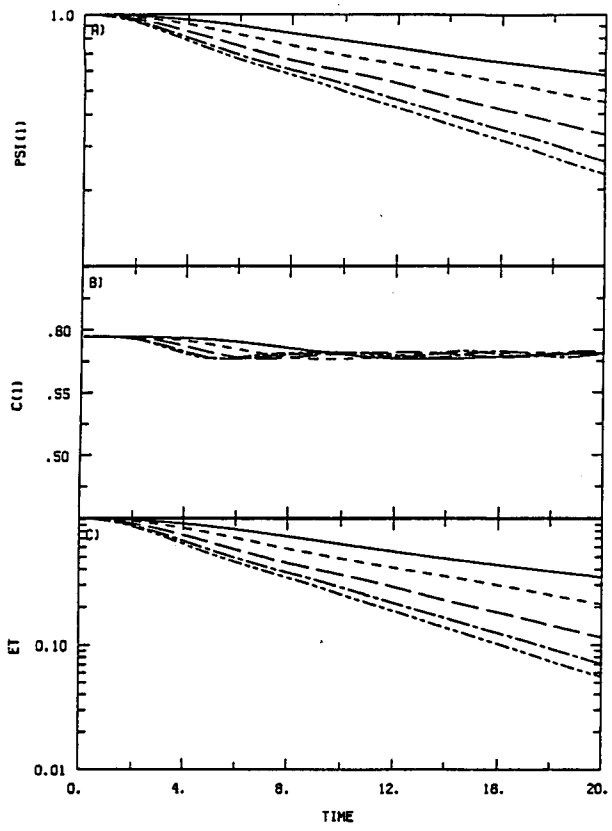


FIG. 6. Time series of (a) $|\tilde{\psi}|^{z=1}$, (b) $c|^{z=1}$, and (c) $E_T$ for initial-value experiments with $\beta = 0.5$, $K^2 = 7.25$, and variable $k$ and $l$. $k = 1$, $l = 2.5$ (solid line), $k = 1.4$, $l = 2.3$ (short-dash line), $k = 1.9$, $l = 1.9$ (long-dash line), $k = 2.3$, $l = 1.4$ (long-dash–short-dash line), and $k = 2.5$, $l = 1$ (long-dash–double short-dash line). Initial streamfunction amplitude is fixed to unity at the lid, and $E_T$ is normalized by its initial value.

section 2d that $\beta = 0.5$ corresponds to an upper bound for midlatitude tropospheric QPV gradients.

### b. *Initial-value experiments*

In this section we perform a series of initial-value experiments with the initial condition consisting of the upper-level edge wave solution for $\beta = 0$. We vary the three parameters, $\beta$, $k$, and $l$, in order to isolate the parameter dependency of the decay rate and propagation speed of the quasi modes.

#### 1) VARYING $\beta$

We vary $\beta$ but keep $k$ and $l$ constant: $k = 2.3$, $l = 1.4$. Figure 2 displays the time series of $|\tilde{\psi}|^{z=1}$, $c|^{z=1}$ (the propagation speed at the lid), and $E_T$ for five different experiments. When $\beta = 0$ (solid line), the streamfunction amplitude at the lid and the perturbation total energy remain constant, while the mode propagates at a fixed rate, $c = 0.6292$ (which is close to the analytical value $c = 0.6286$). As $\beta$ increases, the streamfunction amplitude at the lid decays in time with an exponential behavior (notice the straight lines on log-linear plots). The total perturbation energy evolves similarly but the decay proceeds at a faster rate. Small oscillations around the exponential behavior are visible, especially at $\beta = 1$ (long-dash–short-dash–short-dash line). The propagation speed at the lid lowers as $\beta$ increases, and oscillates in time when $\beta$ becomes large, that is, at $\beta = 0.75$ and $\beta = 1$.

In Fig. 3 we show the time evolution of perturbation fields of streamfunction and QPV for $\beta = 0.5$. At the initial time, the eddy QPV is null in the interior, which is a characteristic of the upper-level edge wave solution. As time marches, the eddy QPV is generated by the advection of $\beta$ by the meridional wind and sheared by the basic-state wind [remember (15)]. It maximizes in the critical region where the flow speed equals the approximate phase speed, that is, around $z = 0.6$ ($c|^{z=1} \approx 0.58$ from Fig. 2b). The streamfunction displays a slight downstream tilt that becomes more and more localized around the critical region as time progresses.

Figure 4 displays perturbation fields $\tilde{\psi}$, $\tilde{q}$, $\tilde{\theta}$, and $\tilde{w}$, for $\beta = 0.5$ at time = 10. It is interesting to compare

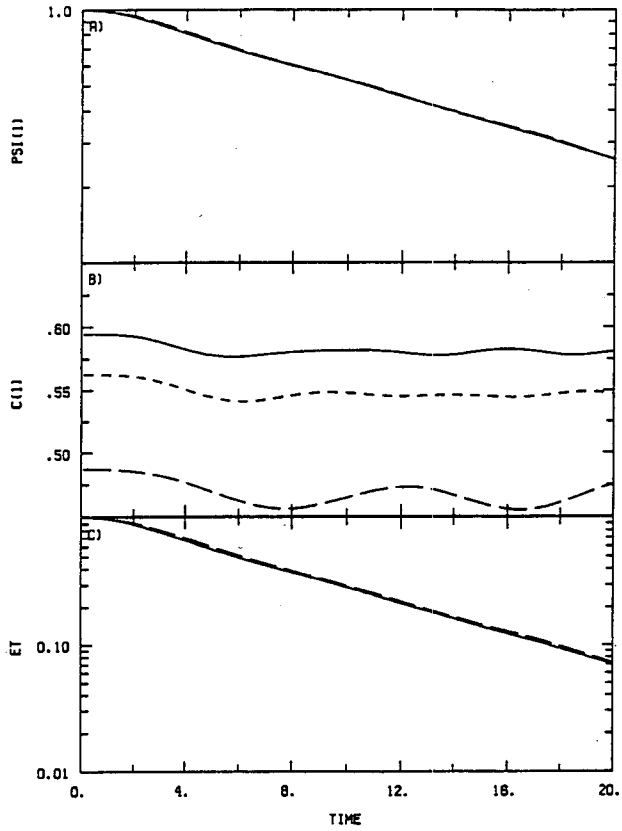


FIG. 7. Time series of (a) $|\tilde{\psi}|^{z=1}$, (b) $c|^{z=1}$, and (c) $E_T$ for initial-value experiments with $\beta = 0.5$, $\beta k/K^2 = 0.159$, and variable $k$ and $l$. $k = 2.3$, $l = 1.4$ (solid line), $k = 2$, $l = 1.518$ (short-dash line), and $k = 1.5$, $l = 1.574$ (long-dash line). Initial streamfunction amplitude is fixed to unity at the lid, and $E_T$ is normalized by its initial value.

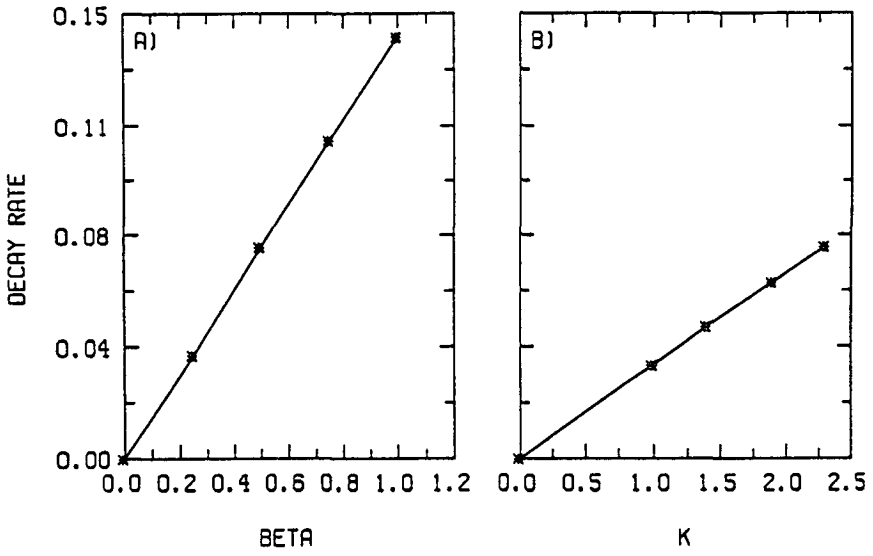


FIG. 8. Dependencies of the decay rate, Λ, evaluated from initial-value experiments, with respect to (a) $\beta$ and (b) $k$. Each star corresponds to a numerical experiment. In (a), results from initial-value experiments with $k = 2.3$ and $l = 1.4$ are displayed, whereas in (b), results from experiments with $\beta = 0.5$ and $K^2 = 7.25$ are shown.

this figure with Fig. 5, which shows the same perturbation fields with the same parameters, but for the lower-level Charney normal mode. The lower-level mode propagates at a phase speed, $c_r = 0.328$, and grows at a fixed rate, $\Omega = kc_i = 0.064$. The streamfunction and vertical velocity fields display upstream tilt with height, which is indicative of a growing mode, while the QPV field shows large downstream tilt around the critical level where it sharply peaks. The perturbation fields of the initial-value experiment are oppositely tilted, with the streamfunction and vertical velocity leaning downshear, but the QPV field still shows downshear tilt in the critical region where it maximizes.

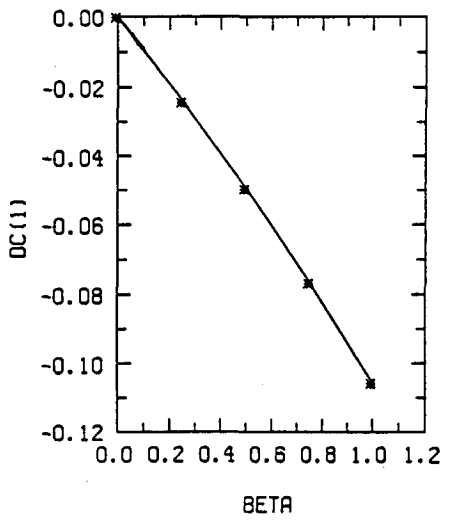


FIG. 9. Dependency of the propagation speed change, $\Delta c|^{z=1}$, evaluated from initial-value experiments, with respect to $\beta$. Each star corresponds to a numerical experiment with $k = 2.3$ and $l = 1.4$.

Even if some of the perturbation fields of initial-value experiments, especially QPV and temperature, do not have fixed structure, decay rate, and phase speed, the fields of streamfunction and vertical velocity show a lot of behaviors typical of modes. The streamfunction field keeps a distinct maximum at the lid, which propagates at a fairly steady rate for small $\beta$. Similarly to the Charney modes that become lower-level Eady modes in the limit of $s, \beta \to 0$, they can be considered as quasi modes that reduce to upper-level Eady modes. This concept will be clarified in section 3c.

### 2) VARYING $k$ AND $l$

We examine the evolution of the initial-value problem varying $k$, but keeping $\beta$ and $(k^2 + l^2)$ constant: $\beta = 0.5$ and $(k^2 + l^2) = 7.25$. Figure 6 shows time series of $|\tilde{\psi}|^{z=1}$, $E_T$, and $c|^{z=1}$ for five different experiments. As $k$ increases, both the streamfunction at the lid and the total perturbation energy decay at faster rates. However, changes in $k$ do not affect the propagation speed at the lid.

We also study the initial-value problem, varying $k$ and $l$, but keeping $\beta$ and $\beta k/(k^2 + l^2)$ constant: $\beta = 0.5$ and $\beta k/(k^2 + l^2) = 0.159$. As shown in Figs. 7a and 7c, the decay of the streamfunction at the lid and of the total perturbation energy proceeds at the same rate for the three experiments. However, the propagation speed at the lid decreases as $(k^2 + l^2)$ decreases.

The results presented so far suggest the parameter dependencies for the decay rate, $\Lambda = g[\beta k/(k^2 + l^2)]$,

and for the propagation speed change, $\Delta c|^{z=1} = f(\beta, (k^2 + l^2))$, where $\Delta c|^{z=1}$ is the propagation speed at the lid minus that of the original edge wave solution.

### 3) THE DECAY RATE AND THE PROPAGATION SPEED CHANGE

We present here approximate expressions for the decay rate and the propagation speed change that can be inferred from initial-value experiments. We are interested in the decay rate of the streamfunction amplitude at the lid and in the propagation speed at the lid. Since the amplitude of perturbation streamfunction maximizes at the lid, we think it is a proper way to characterize the quasi modes.

Let us first evaluate the decay rate $\Lambda$,

$$|\tilde{\psi}|^{z=1} = |\tilde{\psi}|^{z=1,t=0} e^{-\Lambda t}.$$

In initial-value experiments we evaluate $\Lambda$ from the decay that occurs between time = 4 and 20:

$$\Lambda = -\frac{1}{16} \ln\left(\frac{|\tilde{\psi}|^{z=1,t=20}}{|\tilde{\psi}|^{z=1,t=4}}\right).$$

Figures 8a and 8b show that the decay rate depends linearly with $\beta$ and $k$. A linear regression on the five points of Fig. 8a leads to the relation:

$$\Lambda = 0.45 \frac{\beta k}{(k^2 + l^2)}, \qquad (29)$$

where the correlation coefficient is greater than .999. A regression on the five points of Fig. 8b leads to the same result within one percent. The relationship (29) holds for the parameter range explored in initial-value experiments: $0 < \beta < 1$, $0 < k < 2.5$, and $4.7 < (k^2 + l^2) < 7.3$. It is interesting to compare this rate with the approximate decay rate in the normal-mode limit

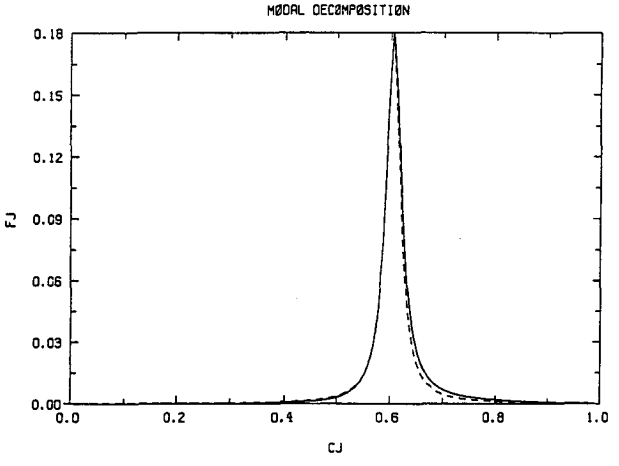


FIG. 10. Distribution $F_j$ as a function of $c_j$, for an initial-value experiment with $\beta = 0.25$, $k = 2.3$, and $l = 1.4$ (solid line), and for an idealized distribution of the form (32) with parameters specified in the text (dash line).

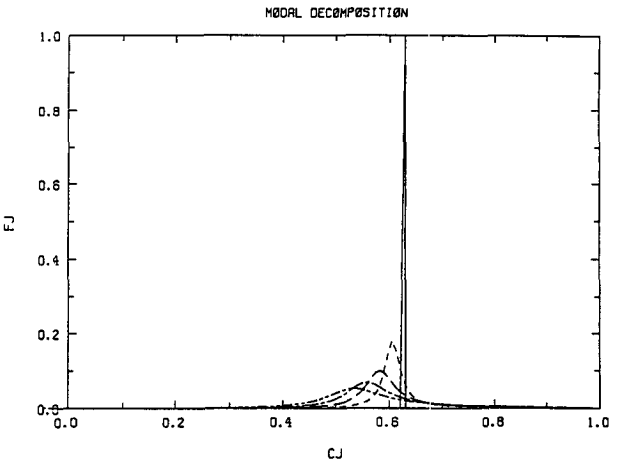


FIG. 11. Distributions $F_j$ as a function of $c_j$, for initial-value experiments with $k = 2.3$ and $l = 1.4$. $\beta = 0$ (solid line), 0.25 (short-dash line), 0.5 (long-dash line), 0.75 (long-dash–short-dash line), and 1 (long-dash–double short-dash line).

$\Lambda_n$, evaluated in section 4 of P1. The approximation derived in P1 does very well: the parameter dependency is the same and the rate is slightly smaller than the rate of initial-value experiments. The initial-value experiments show that nothing singular happens at the critical level even if a maximum of $|\tilde{q}|$ is generated in the region.

Now we evaluate the change in propagation speed at the lid. It is obvious in the initial-value experiments that the propagation speed at the lid fluctuates with time, especially at large horizontal scales, that is, small $(k^2 + l^2)$ and large $\beta$. We solve this problem by calculating average of $c|^{z=1}$ from time = 4 to 20 for each experiment. We then compute $\Delta c|^{z=1}$ by subtracting from the average the numerical value of the phase speed of the edge wave solution, $c = 0.6292$. Figure 9 displays the dependency of $\Delta c|^{z=1}$ with respect to $\beta$. A linear regression using the five points of Fig. 9 yields the relation:

$$\Delta c|^{z=1} = -0.105\beta, \qquad (30)$$

where the correlation coefficient is greater than 0.999. The linear relation (30) is valid in the parameter range $0 < \beta < 1$, $0 < k < 2.5$, and $(k^2 + l^2) = 7.25$.

In the extratropical atmosphere a realistic upper-bound value for tropospheric $Q_y$ corresponds to $\beta = 0.5$. For $k = 2.3$ and $l = 1.4$, which correspond to a channel width of 2000 km and a zonal wavelength of 2500 km, the streamfunction amplitude at the lid decays by an exponential factor in $t_d = \Lambda^{-1}$, 14 time units (dimensionally 5.5 days), and the propagation speed is $c|^{z=1} = 0.58$ (dimensionally 15.6 m s$^{-1}$).

### c. *Propagating quasi modes in shear*

In this section we clarify the mathematical description of quasi modes. Neither neutral nor unstable

modes are supported by the basic states studied in this section. However, they support decaying quasi modes that consist of a superposition of singular modes sharply peaked in the phase speed domain.

The solution to the initial-value problem can be expressed as in (28):

$$\tilde{\psi}(z, t) = \sum_{j=1}^{N} a_j \hat{\psi}_j e^{-ikc_j t},$$

where

$$a_j = \frac{(\hat{\psi}_j^a, \psi_E)}{(\hat{\psi}_j^a, \hat{\psi}_j)}$$

and where $\psi_E$ represents the upper-level wave solution at a certain truncation. In this section we are interested specifically at the time evolution of the streamfunction amplitude at the lid:

$$\tilde{\psi}(1, t) = \sum_{j=1}^{N} F_j e^{-ikc_j t}, \tag{31}$$

where

$$F_j = a_j \hat{\psi}_j(1).$$

Let us examine two distributions $F_j$ that lead to analytical solutions to (31). First, we study a case with uniform $F_j$,

$$F_j = \begin{cases} 1, & \text{in the domain } [c_1, c_2] \\ 0, & \text{elsewhere.} \end{cases}$$

Then, changing the summation for an integral in (31) yields

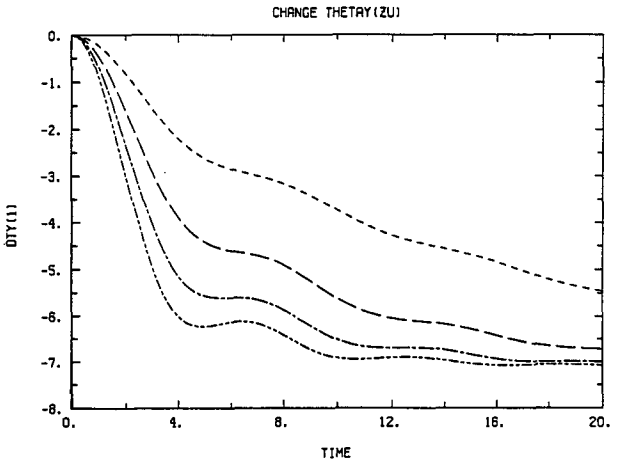


FIG. 12. Time series of changes in the midchannel-mean temperature gradient at the lid for initial-value experiments with $k = 2.3$ and $l = 1.4$. $\beta = 0.25$ (short-dash line), 0.5 (long-dash line), 0.75 (long-dash–short-dash line), and 1 (long-dash–double short-dash line). The initial streamfunction amplitude at the lid is fixed to unity in each experiment.

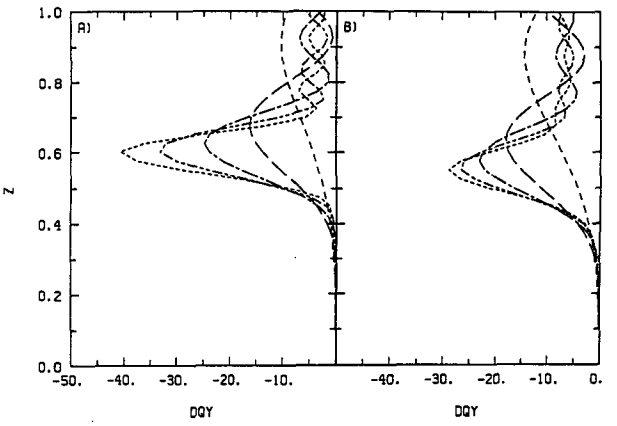


FIG. 13. Time evolution of the vertical profiles of changes in the midchannel QPV gradient for initial-value experiments with $k = 2.3$ and $l = 1.4$. (a) $\beta = 0.5$ and (b) $\beta = 1$. Time = 4 (short-dash line), 8 (long-dash line), 12 (long-dash–short-dash line), 16 (long-dash–double short-dash line), and 20 (very small dash line). The initial streamfunction amplitude at the lid is fixed to unity in each experiment.

$$\hat{\psi}(1, t) = \int_{c_1}^{c_2} dc e^{-ikct}$$

$$= \frac{2}{kt} \exp\left[-ik\left(\frac{c_1 + c_2}{2}\right)t\right] \sin k\left(\frac{c_2 - c_1}{2}\right)t.$$

The streamfunction decays as $1/t$, a result consistent with the more general results of Case (1960).

Let $F_j$ take the following form,

$$F_j = \frac{\mathcal{H}}{(c_j - c_0)^2 + w^2}, \tag{32}$$

where $c_0$ is the location of the peak and $w$ the half-width. After changing the summation to an integral in (31), and assuming that $F_j$ has significant values only in the range of phase speeds supported by the basic state, we arrive at the expression,

$$\tilde{\psi}(1, t) = \int_{-\infty}^{\infty} dc \frac{\mathcal{H} e^{-ikct}}{(c - c_0)^2 + w^2}.$$

A change of variable, $c' = c - c_0$, yields

$$\tilde{\psi}(1, t) = \mathcal{H} e^{-ikc_0 t} \int_{-\infty}^{\infty} dc' \frac{e^{-ikc't}}{c'^2 + w^2}$$

$$= \frac{\mathcal{H}\pi}{w} e^{-ikc_0 t} e^{-wkt}.$$

The streamfunction wave at the lid propagates with speed $c_0$ and decays exponentially at a rate, $\Lambda = wk$. The decay proceeds as the singular modes interfere with one another.

These two examples can help to clarify the concept of a quasi mode as a sharply peaked distribution of singular modes. When the distribution is sharply

peaked, the decay of the streamfunction does not proceed as $1/t$, thus depending only on the shear, but proceeds at a rate determined by the width of the peak. Quasi modes behave essentially as slowly decaying modes.

Figure 10 displays the distribution $F_j$ for an initial-value experiment with $\beta = 0.25$ (solid line), and $F_j$ calculated from expression (32) (dash line). In (32) the parameters are fixed by the results of initial-value experiments presented in section 3b. From these the decay rate, $\Lambda$, and the propagation speed change, $\Delta c|^{z=1}$, are known. We can then compute $c_0$ by adding $\Delta c|^{z=1}$ to the phase speed of the original edge wave solution, 0.6292, and $w$ with the expression $w = \Lambda/k$. The two distributions are remarkably similar. Therefore, it is not surprising that initial-value experiments display the exponential decay of the streamfunction at the lid (recall Fig. 2; the dash line corresponds to the case illustrated in Fig. 10).

Figure 11 displays the distributions $F_j$ for different values of $\beta$. When $\beta = 0$, the distribution is simply a Kronecker delta (solid line). As $\beta$ increases, the distribution $F_j$ widens, and its peak moves toward smaller phase speeds. Notice that it also becomes more asymmetrical with respect to the peak, with amplitudes larger on the side of larger phase speeds.

### d. *Wave–mean-flow interaction*

We examine in this section the effect of decaying quasi modes on the mean flow, where the mean refers to the zonal average. We more specifically look at the temperature gradient at the upper boundary, $\bar{\Theta}_y$ $(y, z = 1, t)$, and at the vertical profiles of meridional QPV gradient, $\bar{Q}_y(y, z, t)$. These two relations hold:

$$\frac{\partial(\bar{\Theta}_y|^{z=1}}{\partial t} = -l^2 RE[(\tilde{v}\tilde{\theta}^*|^{z=1}] \cos 2ly, \quad (33)$$

$$\frac{\partial \bar{Q}_y}{\partial t} = -l^2 RE[\tilde{v}\tilde{q}^*] \cos 2ly. \quad (34)$$

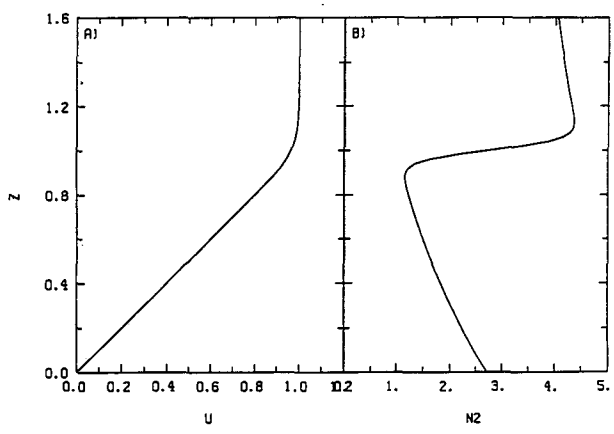


FIG. 14. The vertical profiles of basic-state (a) wind $U(z)$ and (b) stability $N^2(z)$.

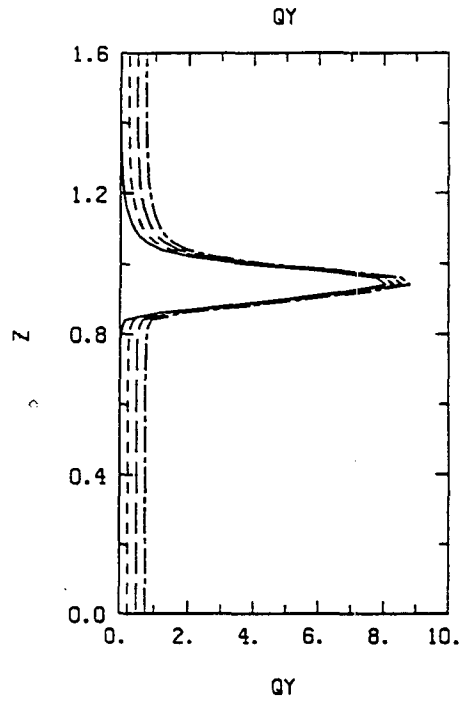


FIG. 15. The vertical profiles of basic-state QPV gradient, $Q_y$. $\beta = 0$ (solid line), 0.25 (short-dash line), 0.5 (long-dash line), and 0.75 (long-dash–short-dash line).

Also from this integral relationship,

$$(\overline{v\theta}|^{z=1} = \int_{-\infty}^{1} dz\overline{vq}, \quad (35)$$

we must also have

$$\frac{\partial(\bar{\Theta}_y|^{z=1}}{\partial t} = \int_{-\infty}^{1} dz \frac{\partial \bar{Q}_y}{\partial t}.$$

When the wave transports heat southward at the upper boundary, $RE[(\tilde{v}\tilde{\theta}^*|^{z=1}] < 0$, the magnitude of the temperature gradient (which is negative) increases in the middle of the channel and decreases on its sides. When the wave transports QPV southward, $RE[\tilde{v}\tilde{q}^*] < 0$, the gradient $\bar{Q}_y$ is enhanced at the sides of the channel, but decreased in its middle.

Figure 12 depicts changes in the midchannel-mean temperature gradient at the lid induced by quasi modes for initial-value experiments with parameters as in Fig. 2. Each curve represents a different value of $\beta$: $\beta = 0.25$, 0.5, 0.75, 1.0, while $k$ and $l$ are fixed to 2.3 and 1.4. The magnitude of the midchannel-mean temperature gradient at the lid increases as quasi modes decay. This enhancement proceeds at a rate that increases as $\beta$ increases. Remember that it is accompanied by a reduction of the gradient on the sides of the channel [see (33)].

We show changes in the midchannel mean QPV gradient for initial-value experiments with $\beta = 0.5$ and

$\beta = 1$ in Fig. 13. Each curve refers to a different time in the simulation. The large numbers present in the abscissas of Fig. 13 are due to the fact that in the initial-value experiments the initial streamfunction amplitude at the lid is fixed to unity (this is also the case in Fig. 12). For both cases, the "quasi mode" acts to erase basic-state QPV gradients that are positive. As time progresses, the largest changes occur in the critical region. When $\beta = 1$, changes do not become as sharply peaked as when $\beta = 0.5$. The quasi mode simultaneously induces an increase in the mean QPV gradient on the sides of the channel [recall (34)].

It is interesting to evaluate a time scale for the decay of the interior QPV gradients due to upper-level waves. Let us consider realistic values for the parameters and for the perturbation amplitude. To calculate a time scale we consider an initial perturbation amplitude of $|\tilde{\psi}|^{z=1,t=0} = 0.2$, $\beta = 0.5$, $k = 2.3$, and $l = 1.4$. These numbers correspond to an initial perturbation of 5 dm and 12 m s$^{-1}$ at the tropopause, with a zonal wavelength of 2500 km and a channel width of 2000 km. For these parameter values, from Fig. 13a, the mid-channel-mean QPV gradients in the critical region are destroyed after 8 time units (dimensionally 3.1 days).

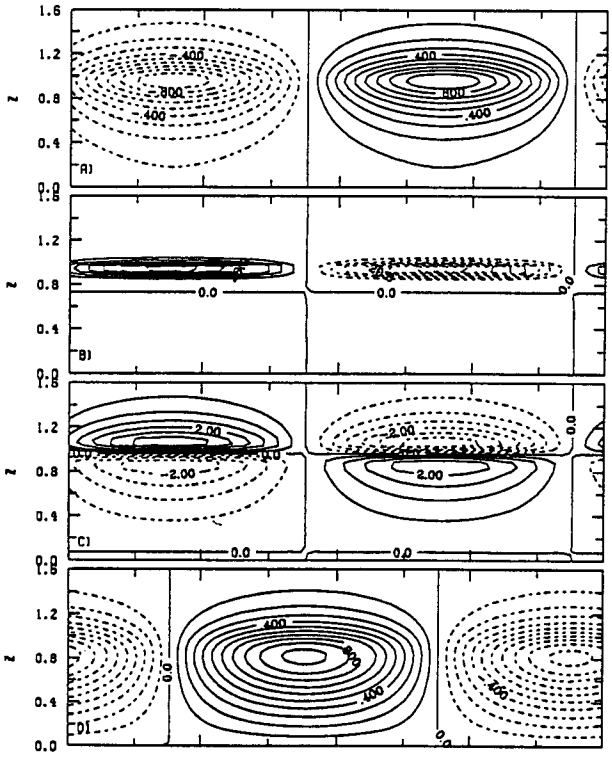


FIG. 16. Midchannel $x$–$z$ cross section of perturbation fields for the upper-level normal mode at $k = 2.3$, $l = 1.4$, and $\beta = 0.0$. (a) Streamfunction, (b) QPV, (c) potential temperature, and (d) vertical velocity. The contour interval is 0.1 in (a), 5 in (b), 0.5 in (c), and 0.1 in (d). Negative values are dashed. A full zonal wavelength is represented.

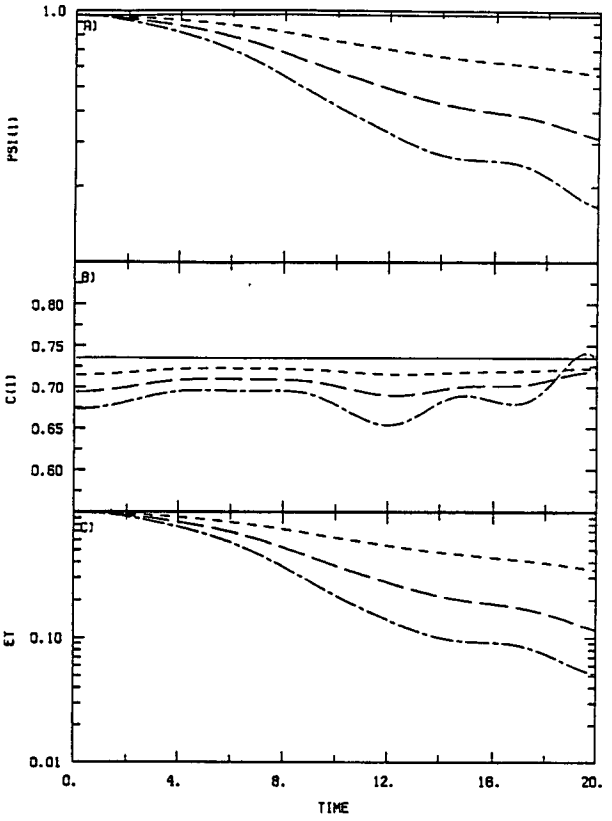


FIG. 17. Time series of (a) $|\tilde{\psi}|^{z=1}$, (b) $c|^{z=1}$, and (c) $E_T$ for initial-value experiments with $k = 2.3$, $l = 1.4$, and variable $\beta$. $\beta = 0$ (solid line), 0.25 (short-dash line), 0.5 (long-dash line), and 0.75 (long-dash–short-dash line). The initial condition consists of the upper-level normal mode for the basic state with zero $\beta$. Initial streamfunction amplitude is fixed to unity at the tropopause, and $E_T$ is normalized by its initial value.

This is accompanied by a doubling in the mean QPV gradient on the sides of the channel. Also, from Fig. 12 (the large-dash line represents the case with $\beta = 0.5$), the mean temperature gradient at the lid is then increased by one-fifth in the middle of the channel, and decreased by the same amount on the sides.

### *e. Discussion*

In this section we showed that the upper-level Eady normal modes have counterparts as decaying quasi modes in models with interior tropospheric QPV gradients. The quasi modes consist of a distribution of singular modes sharply peaked in the phase speed domain, and their decay proceeds as the singular modes present interfere with one another. The concept of quasi modes is important since quasi modes represent a manner by which perturbation energy can be maintained in shear flows, not for an infinite time as for neutral normal modes, but for a sufficient time to be of dynamical relevance.

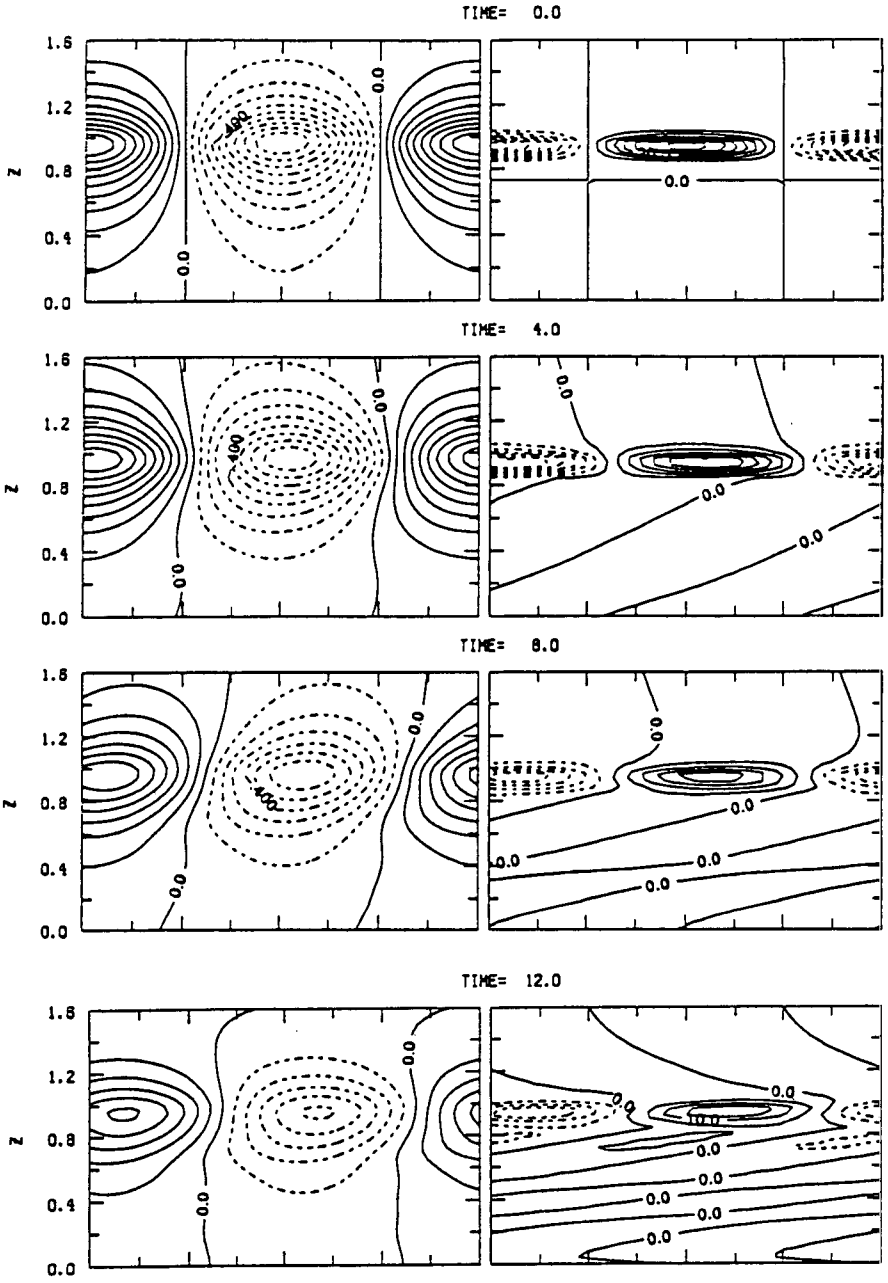


FIG. 18. Time evolution of the midchannel perturbation streamfunction and QPV fields for the initial-value experiment with $k = 2.3$, $l = 1.4$, and $\beta = 0.5$. Time = 0 (a), 4 (b), 8 (c), 12 (d). The initial condition consists of the upper-level normal mode for the basic state with zero $\beta$. The contour interval is 0.1 for the streamfunction, and 5 for the QPV. Negative values are dashed. A full zonal wavelength is represented.

For parameter values typical of synoptic-scale waves at midlatitudes and for a realistic upper-bound value of tropospheric QPV gradients, the quasi modes were found to have marginal decay rates that correspond to exponential decay times of six days. Furthermore, our results show that quasi modes act to erase the critical region mean QPV gradients over time scales of a few days, enhancing the mean temperature gradient at the lid. Their effect on the mean flow is to create a mean flow that further supports them. These results suggest that perturbation energy can indeed be maintained at the tropopause even in the presence of initial interior tropospheric QPV gradients. Sanders (1988) found that the life duration of upper-level mobile troughs at midlatitudes is typically 12 days. While our decay time scale of 6 days may seem too small to account for the

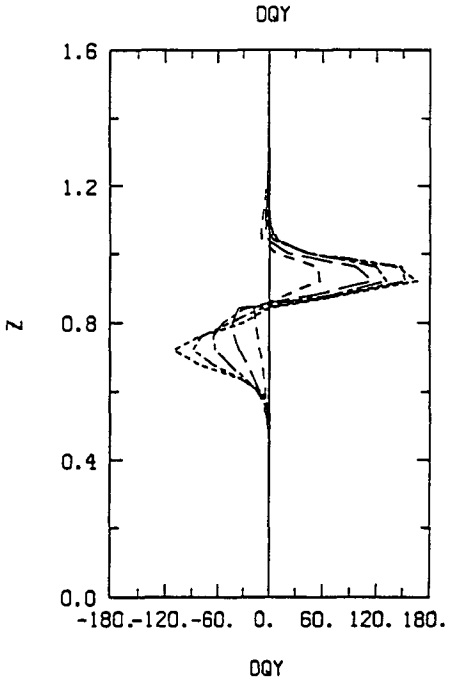


FIG. 19. Time evolution of the vertical profiles of changes in the midchannel QPV gradient for the initial-value experiment with $k = 2.3$, $l = 1.4$, and $\beta = 0.5$. Time = 4 (short-dash line), 8 (long-dash line), 12 (long-dash–short-dash line), 16 (long-dash–double short-dash line), and 20 (dot–dash line). The initial condition consists of the upper-level normal mode for the basic state with zero $\beta$. The initial streamfunction amplitude at the tropopause is fixed to unity.

observations, nonlinear eddy transports were found to erase $Q_y$ in the middle of the channel after 3 days and may be responsible for the long duration of the observed waves.

## 4. Excitation of the quasi modes

### a. *Basic states*

We assume in this section a semi-infinite atmosphere with a rigid lower boundary at $z = 0$. The density decays exponentially with height at a constant rate, $s = 1$. The basic-state wind takes the following form,

$$z < z_t - \delta_u, \quad U(z) = z,$$

$$z > z_t - \delta_u,$$

$$U(z) = (z_t - \delta_u) + \delta_u \tanh\left(\frac{z - (z_t - \delta_u)}{\delta_u}\right).$$

We set the tropopause height to unity, $z_t = 1$, and $\delta_u = 0.15$. The static stability profile is

$$N^2(z) = \left(\frac{N_1^2 + N_2^2}{2}\right)\left[1 + \tanh\left(\frac{z - z_t}{\delta_N}\right)\right] + N_1^2(e^{-s(z-z_t)} - 1).$$

We fix the tropospheric and stratospheric static stability: $N_1^2 = 1$ and $N_2^2 = 4.5$, and $\delta_N = 0.05$. For these profiles of wind and static stability, all basic-state quantities that enter the equations to be solved are continuous, because $N^2$ and all its derivatives are continuous, and $U$ and its first and second derivatives are also continuous. Figure 14 displays the vertical profiles of $U$ and $N^2$. From Table 1 these nondimensional values correspond to a maximum stratospheric wind of 27 m s$^{-1}$, with a temperature change across the channel, which varies from 18°C at the ground to zero in the stratosphere, and to a static stability, which varies from $2.7 \times 10^{-4}$ s$^{-2}$ at the ground to $1.5 \times 10^{-4}$ s$^{-2}$ in the upper troposphere, and to $4 \times 10^{-4}$ s$^{-2}$ in the stratosphere. Note the increased stability close to the ground that is characteristic of the extratropical atmosphere where lapse rates at lower levels are generally smaller than at upper levels.

The vertical profiles of $Q_y$ for different values of $\beta$ are shown in Fig. 15. It strongly peaks at the tropopause and reduces to $\beta$ in the troposphere and stratosphere. The temperature gradient at the lower boundary is equivalent to a thin sheet of large negative $Q_y$ (Bretherton 1966). The necessary condition for normal-mode

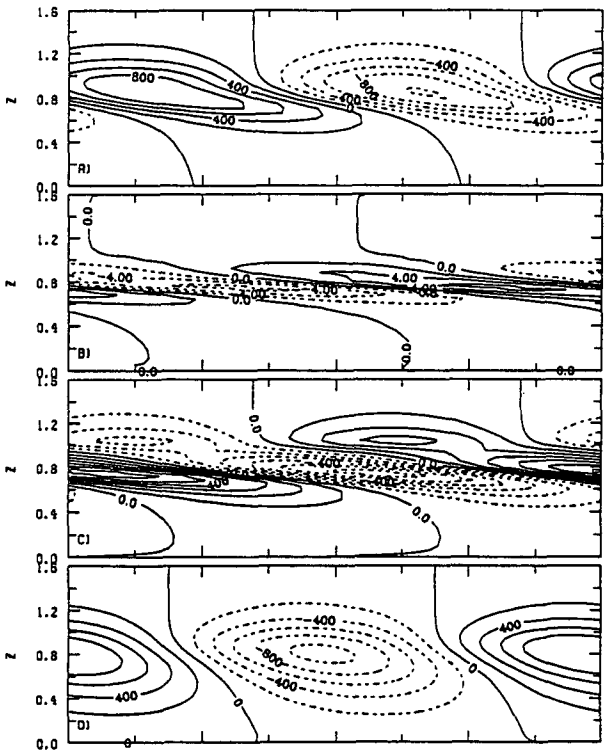


FIG. 20. Midchannel $x$–$z$ cross section of the perturbation fields for the near-optimal initial condition at $k = 2.3$, $l = 1.4$, and $\beta = 0$, for $\epsilon = 0.15$. (a) Streamfunction, (b) QPV, (c) potential temperature, and (d) vertical velocity. The contour interval is 0.02 in (a), 2 in (b), 0.1 in (c), and 0.02 in (d). Negative values are dashed. A full zonal wavelength is represented.

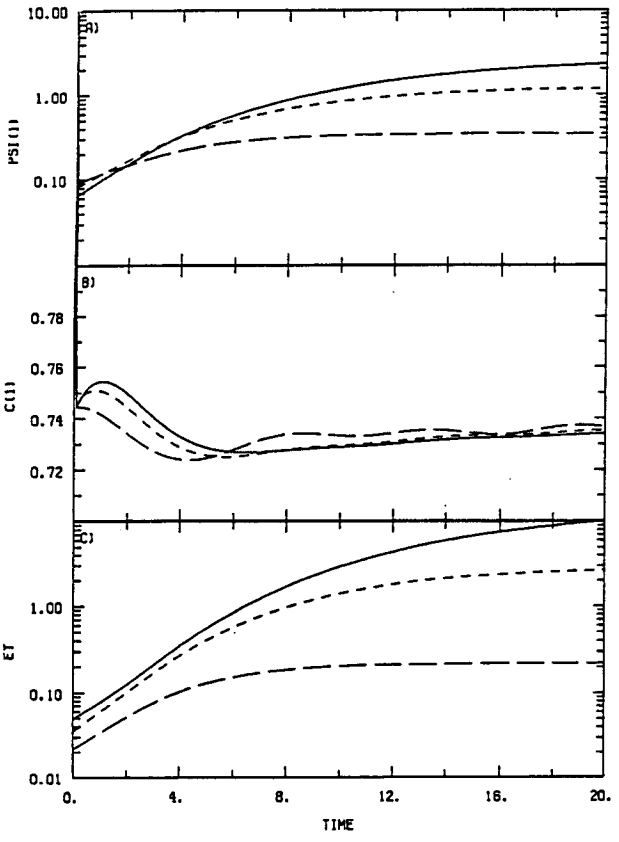


FIG. 21. Time series of (a) $|\tilde{\psi}|^{z=1}$, (b) $c|^{z=1}$, and (c) $E_T$ for initial-value experiments with $k = 2.3$, $l = 1.4$, $\beta = 0$, and variable $\epsilon$. $\epsilon = 0.1$ (solid line), 0.15 (short-dash line), and 0.3 (long-dash line). The initial conditions consist of the near-optimal disturbances for the basic state with zero $\beta$.

instability of the Charney–Stern theorem is then satisfied. In this section we consider fixed zonal and meridional wavenumbers, $k = 2.3$ and $l = 1.4$, which correspond to a zonal wavelength of 2500 km and to a channel width of 2000 km. At that horizontal scale the basic state with $\beta = 0$ does not support any normal-mode instability; when $0 < \beta < 1$, however, low-level modes of marginal instability exist.

### b. *The upper-level wave solutions*

Figure 16 displays the character of the neutral upper-level normal-mode solution for the basic state with $\beta = 0$; perturbation streamfunction, QPV, potential temperature, and vertical velocity fields are shown. Unlike the upper-level normal-mode solution shown in Part I, Fig. 9, the perturbation QPV and $\theta$ fields in Fig. 16 are continuous at the tropopause. The upper-level wave solution displayed in Fig. 16 propagates at a phase speed, $c = 0.73$.

In a series of initial-value experiments that resemble those performed in section 3, we examine what happens to the neutral upper-level wave solution in the presence of stratospheric and tropospheric $Q_y$. Figure 17 displays the time series of $|\psi|^{z=1}$, $c|^{z=1}$, and $E_T$ for experiments with $\beta = 0$, 0.25, 0.5, and 0.75. When $\beta$ is nonzero, the streamfunction amplitude at $z = 1$ and the total perturbation energy decay with time, and the decay rate increases as $\beta$ increases. The propagation rate at the tropopause decreases as $\beta$ increases. At $\beta = 0.5$, the exponential decay rate for the streamfunction amplitude at $z = 1$ is 0.064, which corresponds to a time scale of 16 units (dimensionally 6.1 days). This decay time scale compares well with that of 5.5 days found in section 3 at $\beta = 0.5$ for the same horizontal scale.

Figure 18 displays the time evolution of $\tilde{\psi}$ and $\tilde{q}$, for $\beta = 0.5$. At the initial time the streamfunction field corresponds to the neutral upper-level wave solution. The phase lines are vertical. At later time, eddy QPV is generated in the stratosphere and the troposphere, and the streamfunction field acquires a downshear tilt in the troposphere. The magnitudes of the QPV and streamfunction extrema at the tropopause decrease, and another extremum in the QPV field is generated in the critical region below the tropopause, around $z = 0.7$. This time evolution is very similar to that represented in Fig. 3, which depicts the case with a rigid tropopause and no lower boundary. The results of section 3 are robust, and hold in the presence of the ground and the stratosphere. Figure 19 depicts the change in QPV gradient, $\Delta Q_y(z)$, induced by the wave transport. In the middle of the channel the wave acts to erase the gradients in the critical region around $z = 0.7$, and to enhance the gradients above around $z = 0.9$.

In the initial-value experiments with $\beta > 0$ presented in this section, we do not observe a rapid development of lower-level waves. The presence of enhanced stability at the ground causes the lower-level waves to be only marginally unstable. For instance at $\beta = 0.5$, their growth rate is 0.027, which corresponds to an exponential time scale of 15.9 time units (dimensionally, 6.2 days).

### c. *Excitation from favorable initial conditions*

Farrell (1989) found that the adjoint of a given mode is the optimal perturbation to excite that mode in the total perturbation energy ($E_T$) norm. We calculate near-optimal initial conditions for the upper-level wave solution when $\beta$ is zero:

$$\tilde{\psi}_{no} = \frac{\hat{\psi}_{UL}}{U(z) - (c_{UL} - i\epsilon)}, \tag{36}$$

TABLE 2. Magnifications for a basic state with $\beta = 0$.

| $\epsilon$ | $\lvert\tilde{\psi}\rvert^{z=1,\max}/\lvert\tilde{\psi}\rvert^{z=0,t=0}$ | $E_T^{\max}/E_T^{t=0}$ |
|---|---|---|
| .1 | 35.8 | 205.3 |
| .15 | 14.5 | 74.1 |
| .3 | 3.7 | 10.3 |

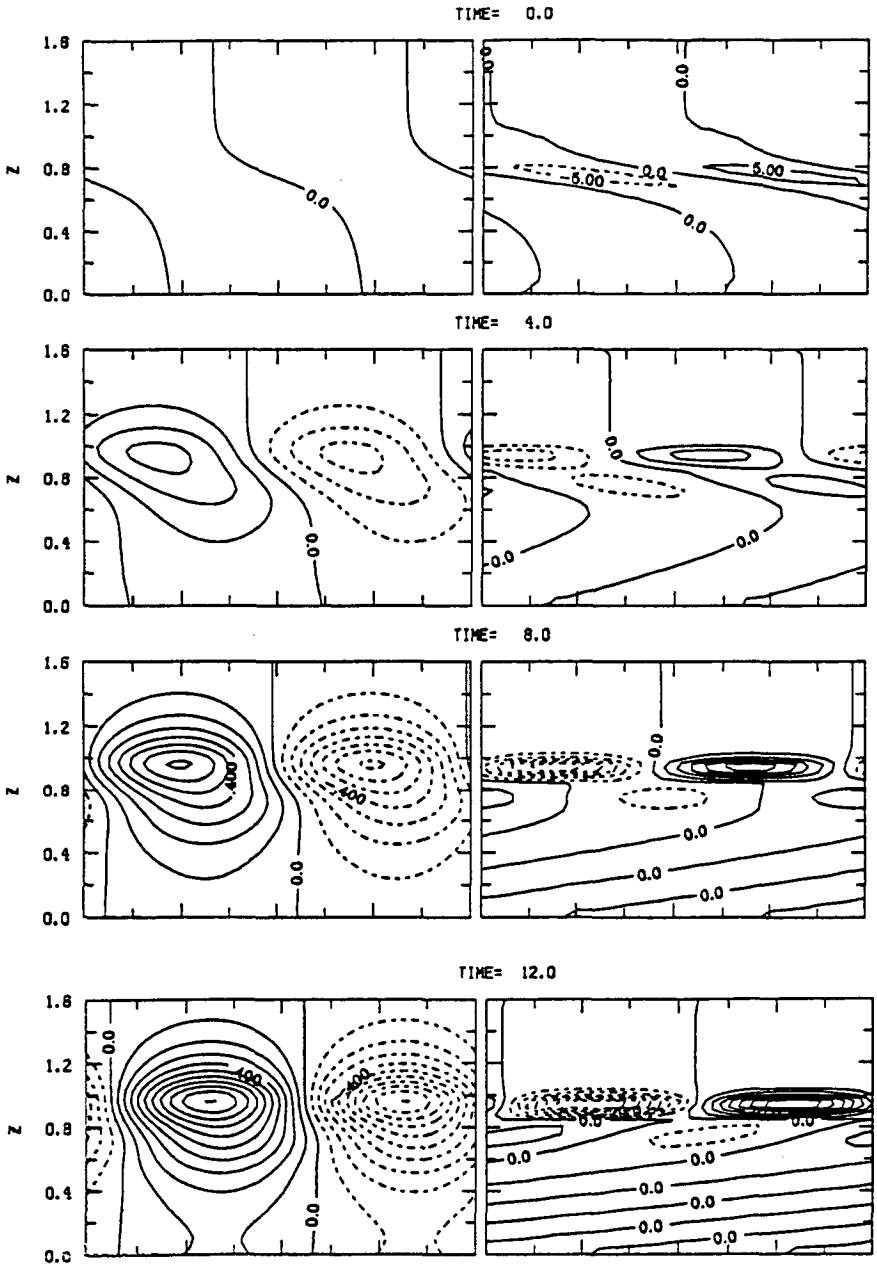


FIG. 22. Time evolution of the midchannel perturbation streamfunction and QPV fields for the initial-value experiment with $k = 2.3$, $l = 1.4$, $\beta = 0$, and $\epsilon = 0.15$. Time = (a) 0, (b) 4, (c) 8, (d) 12. The initial condition consists of the near-optimal disturbance for the basic state with zero $\beta$. The contour interval is 0.1 for the streamfunction, and 5 for the QPV. Negative values are dashed. A full zonal wavelength is represented.

as in Montgomery and Farrell (1990). Here $\hat{\psi}_{UL}$ and $c_{UL}$ are the streamfunction field and the phase speed associated with the upper-level mode for basic state with $\beta = 0$; $\epsilon$ is an arbitrary factor that controls the amount by which the perturbation fields lean against the shear. When $\epsilon = 0$, $\tilde{\psi}_{no}$ is the adjoint of the mode and would be the optimal perturbation for the purpose of exciting $\hat{\psi}_{UL}$ in the $E_T$ norm for basic states with constant stability and density. The fact that $c_{UL}$ is real for strictly neutral modes causes these adjoint modes to be singular. For that reason, we consider here resolvable near-optimal excitations with $\epsilon = 0.1$, 0.15, and 0.3.

Figure 20 displays the character of the near-optimal initial condition for an intermediate value of $\epsilon$, $\epsilon = 0.15$; perturbation streamfunction, QPV, temperature, and

vertical velocity fields are shown. All fields possess a pronounced maximum amplitude just below the tropopause and a marked upshear tilt with height. From Table 1, a height perturbation of 1 dm would have associated temperature and vertical velocity perturbations of 2 K and 0.4 cm $s^{-1}$.

When $\epsilon$ is smaller, the disturbances possess a larger amount of upshear tilt and are more concentrated around the critical level of the upper-level neutral normal mode [recall (36)]. Also for equal amplitudes in the streamfunction and vertical velocity fields, they have stronger amplitudes in the QPV and temperature fields. Since the excitation of the upper-level mode takes place as the shear acts on the initial condition, near-optimal conditions with smaller $\epsilon$ and larger amount of upshear tilt lead to longer excitation times and larger growths. For values of $\epsilon$ considered here, 0.1, 0.15, and 0.3, the excitation time scales are approximately of 15, 10, and 5 time units (dimensionally, 6, 4, and 2 days).

Let us now examine the excitation on a basic state with $\beta = 0$, which supports an upper-level normal mode. Figure 21 shows the time evolution of $|\psi|^{z=1}$, $c|^{z=1}$, and $E_T$ for near-optimal initial conditions with different values of $\epsilon$. The streamfunction amplitude at $z = 1$ and the total perturbation energy first increase with time and then remain constant. When $\epsilon$ is smaller, the growth is larger and takes longer to occur. Table 2 contains the magnifications in $|\psi|^{z=1}$ and $E_T$ for the different experiments. At $\epsilon = 0.15$ the amplitude is magnified by a factor of 15 and the energy by 74. Figure 22 displays the time evolution of the streamfunction and QPV fields for $\epsilon = 0.15$. The shear acts on the initially tilted disturbance and excites the upper-level normal mode.

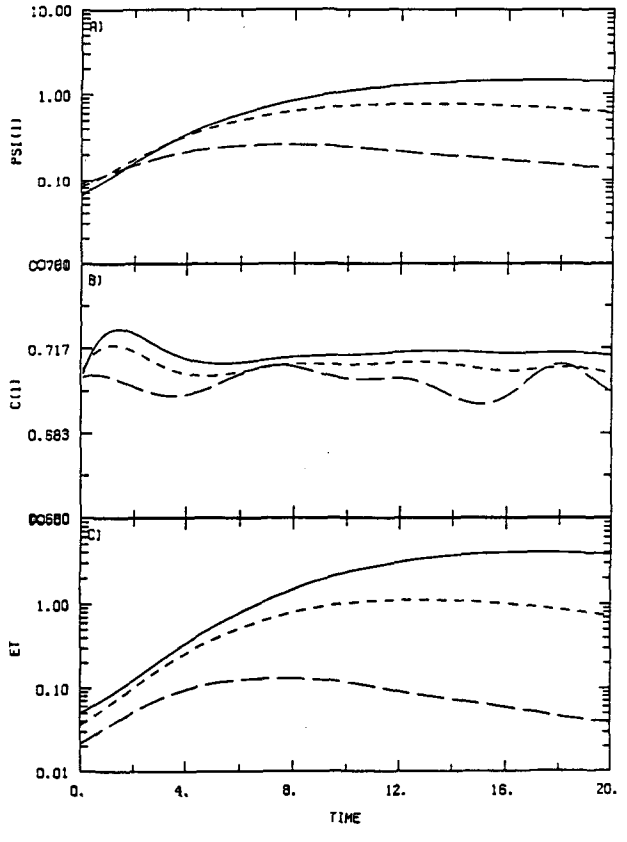


FIG. 23. Time series of (a) $|\tilde{\psi}|^{z=1}$, (b) $c|^{z=1}$, and (c) $E_T$ for initial-value experiments with $k = 2.3$, $l = 1.4$, $\beta = 0.5$, and variable $\epsilon$. $\epsilon = 0.1$ (solid line), 0.15 (short-dash line), and 0.3 (long-dash line). The initial conditions consist of near-optimal disturbances for the basic state with zero $\beta$.

TABLE 3. Magnifications for a basic state with $\beta = 0.5$.

| $\epsilon$ | $\lvert\tilde{\psi}\rvert^{z=1,\max}/\lvert\tilde{\psi}\rvert^{z=0,t=0}$ | $E_T^{\max}/E_T^{t=0}$ |
|---|---|---|
| .1 | 22.4 | 81.1 |
| .15 | 9.4 | 31.2 |
| .3 | 2.9 | 6.1 |

We now examine the same excitation but on a basic state with $\beta = 0.5$, which does not support an upper-level normal mode but rather a quasi mode. Figure 23 shows the time evolution of the same diagnostics as in Fig. 21 for this basic state. As in Fig. 21, the streamfunction amplitude and energy initially increase with time, but the excitation is followed by a slow decay. Table 3 contains the magnifications for the basic state with $\beta = 0.5$. At $\epsilon = 0.15$, the amplitude grows by a factor of 9 and the energy by 31. These magnifications are of the same order of magnitude as those for the basic state with zero $\beta$. Figure 24 shows the time evolution of $\tilde{\psi}$ and $\tilde{q}$ for $\epsilon = 0.15$. Even in the absence of an upper-level normal mode, the excitation of the upper-level wave takes place.

### d. Discussion

The first series of results presented in this section confirms the robustness of upper-level synoptic-scale wave solutions. We first showed that the overall characteristics of the neutral upper-level wave solution presented in Part I can be extended to basic states with a continuous tropopause. When $\beta$ is nonzero, we demonstrated that the slow decay of the upper-level wave proceeds as in section 3 even in the presence of a lower boundary and the stratosphere.

The second series of results concerns the excitation of upper-level wave solutions. We identified disturbances concentrated in the upper troposphere with strong upshear tilt as near-optimal conditions for the emergence of upper-level waves. We further showed that the excitation takes place in a similar manner on basic states with zero and nonzero $\beta$. This result is important, since it shows that quasi modes consisting of a superposition of singular modes are as likely to emerge from an initial perturbation as strictly modal waves.

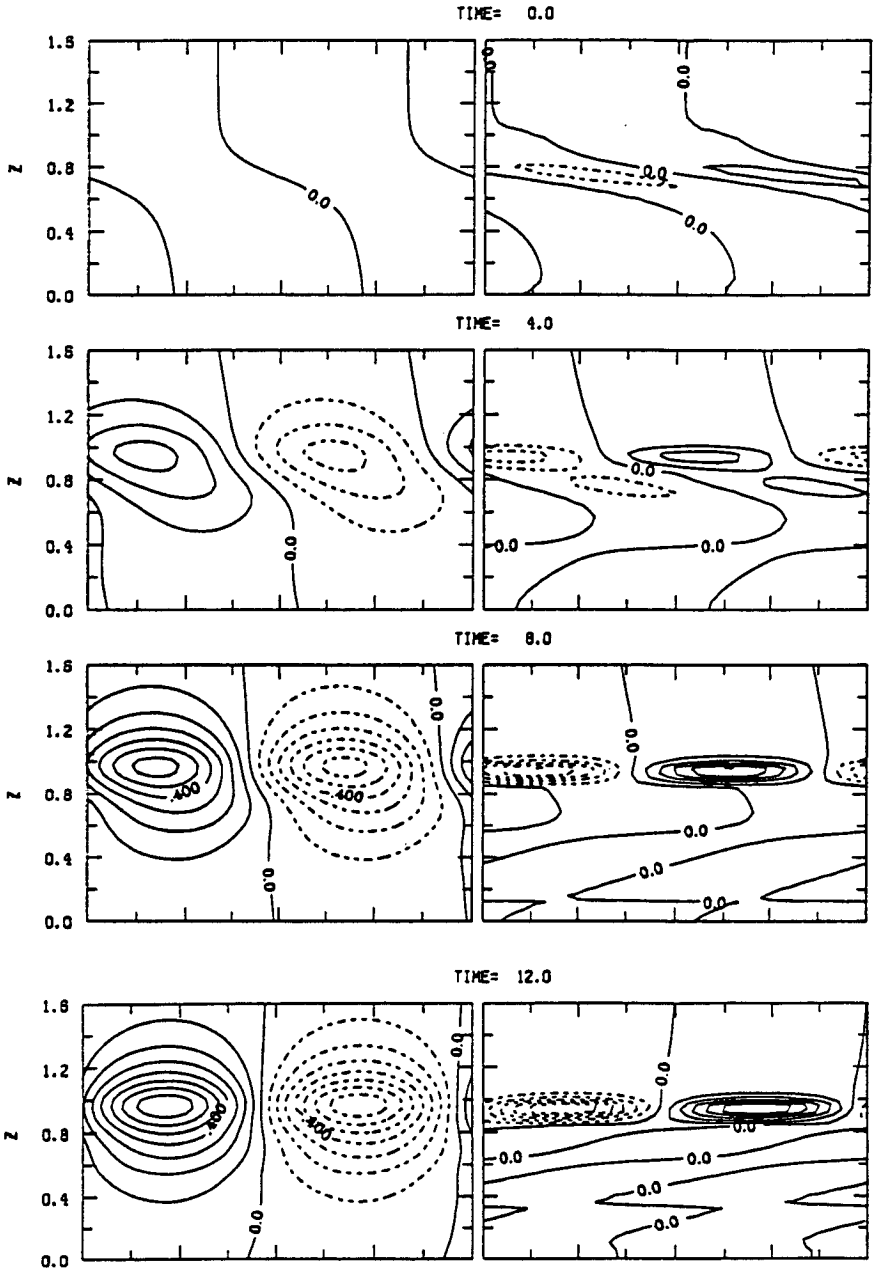


FIG. 24. Time evolution of the midchannel perturbation streamfunction and QPV fields for the initial-value experiment with $k = 2.3$, $l = 1.4$, $\beta = 0.5$, and $\epsilon = 0.15$. Time = (a) 0, (b) 4, (c) 8, (d) 12. The initial condition consists of the near-optimal disturbance for the basic state with zero $\beta$. The contour interval is 0.1 for the streamfunction, and 5 for the QPV. Negative values are dashed. A full zonal wavelength is represented.

## 5. Conclusions

We have shown that counterparts to the Eady normal modes exist in the presence of positive tropospheric gradients of potential vorticity, and that these waves are maintained and excited in a manner similar to that for modal waves. The counterparts of the modes are quasi modes that consist of a distribution of singular modes sharply peaked in the phase speed domain. We have further shown that the nonlinear effects of the quasi modes on the mean flow tends to help their further maintenance.

In summary, the results presented in this paper support identification of the upper-level Eady normal modes as simple models for upper-tropospheric synoptic-scale waves.

*Acknowledgments.* The authors wish to thank Kerry A. Emanuel for many insightful discussions. The first author also thanks Jean-Francois Geleyn for his hospitality at the French Weather Service.

## REFERENCES

Bland, M., and T. Warn, 1975: The radiation condition for transient Rossby waves. *J. Atmos. Sci.*, **32,** 1873–1880.

Bretherton, F. P., 1966: Critical layer instability in baroclinic flows. *Quart. J. Roy. Meteor. Soc.*, **92,** 325–334.

Case, K. M., 1960: Stability of inviscid plane Couette flow. *Phys. Fluids,* **3,** 143–148.

Charney, J. G., and M. E. Stern, 1962: On the stability of internal baroclinic jets in a rotating atmosphere. *J. Atmos. Sci.*, **19,** 159–172.

Eady, E. T., 1949: Long waves and cyclone waves. *Tellus,* **1,** 33–52.

Edmon, H. J., B. J. Hoskins, and M. E. McIntyre, 1980: Eliassen–Palm cross sections for the troposphere. *J. Atmos. Sci.*, **37,** 2600–2616.

Farrell, B., 1982: The initial growth of disturbances in a baroclinic flow. *J. Atmos. Sci.*, **39,** 1663–1686.

——, 1989: On the optimal excitation of baroclinic waves. *J. Atmos. Sci.*, **46,** 668–673.

Green, J. S. A., 1960: A problem in baroclinic stability. *Quart. J. Roy. Meteor. Soc.*, **86,** 237–251.

Held, I. M., 1985: Pseudomomentum and the orthogonality of modes in shear flows. *J. Atmos. Sci.*, **42,** 2280–2288.

Ince, E. L., 1926: *Ordinary Differential Equations.* Reprinted 1956 by Dover, 558 pp.

Lindzen, R. S., B. Farrell, and D. Jacqmin, 1982: Vacillation due to wave interference: Applications to the atmosphere and to the annulus experiments. *J. Atmos. Sci.*, **39,** 14–23.

Montgomery, M. T., and B. F. Farrell, 1990: Dry surface frontogenesis arising from interior potential vorticity perturbations in a semigeostrophic model. *J. Atmos. Sci.*, **47,** 2837–2852.

Pedlosky, J., 1979: *Geophysical Fluid Dynamics.* Springer-Verlag, 624 pp.

Rasch, P. J., 1986: Toward atmospheres without tops: Absorbing upper boundary conditions for numerical models. *Quart. J. Roy. Meteor. Soc.*, **112,** 1195–1218.

Rivest, C., C. A. Davis, and B. F. Farrell, 1992: Upper-tropospheric synoptic-scale waves. Part I: Maintenance as Eady normal modes. *J. Atmos. Sci.*, **49,** 2122–2133.

Rotunno, R., and M. Fantini, 1989: Peterssen's type B cyclogenesis in terms of discrete, neutral Eady modes. *J. Atmos. Sci.*, **46,** 3599–3604.

Sanders, F., 1988: Life history of mobile troughs in the upper westerlies. *Mon. Wea. Rev.*, **118,** 2629–2648.

Snyder, C., and R. S. Lindzen, 1988: Upper-level baroclinic instability. *J. Atmos. Sci.*, **45,** 2445–2459.

Whitaker, J. S., and A. Barcilon, 1992: Genesis of mobile troughs in the upper Westerlies. *J. Atmos. Sci.*, **49,** 2111–2121.